CCD Imager Processing for Backside Illumination Applications*

J. W. Walker B. H. Breazeale L. J. Hornbeck
C. G. Roberts D. P. Stubbs D. R. Collins

Central Research Laboratories, Texas Instruments Incorporated
Dallas, Texas 75265

* This work was supported by NASA/Goddard Space Flight Center under Contract NAS5-22924 and by the Army Night Vision and Electro-optics Laboratories under Contract DAAG53-75-C-0191.

ABSTRACT

The backside illumination of CCD imagers is finding application in the fields of image intensification (for low light level imaging and photon counting), for X-ray imaging, and for optical imaging. Backside illumination requires special chip processing not required otherwise. This processing includes thinning to a 10 micron membrane thickness, boron accumulation at the backside, specialized headers, and specialized bonding techniques. Intensification adds the additional processing associated with vacuum tube and photocathode fabrication. This paper will discuss this processing, presenting data on parameters of interest for each of the above applications.

I. Introduction

The backside illumination of CCD imagers is finding application in the fields of image intensification (for low light level imaging[1] and photon counting[2,3]), for X-ray imaging[4], and for optical imaging[5]. Backside illumination allows the incident radiation to impinge directly onto the silicon. This avoids losses associated with the frontside electrode structure. In addition, it allows the imaging of radiation which otherwise would damage the frontside CCD structure. Backside illumination requires special chip processing not required otherwise.

The fabrication of thinned CCD imagers begins with slices of silicon and progresses through a standard set of processing steps involving photolithography, oxidation, diffusions, metallizations, and etches. The fabrication of a slice of CCD imagers varies little in fundamental detail from the fabrication of other MOS semiconductor devices. However, the remaining processing steps required to produce the final thinned device are nonstandard and require development specifically for backside-illuminated arrays. These remaining processing steps are: (1) thinning, (2) accumulation, and (3) bonding to backside-compatible header. Discussion of these processes follows.

(1) Thinning. CCD imagers are backside illuminated to improve spectral response and to allow electron-bombarded or X-ray operation. These backside-illuminated imagers must be thinned to provide adequate resolution. Resolution is degraded when charge carriers diffuse laterally while diffusing toward the CCD storage wells. The degradation is maximum for radiations absorbed near the silicon surface. Thinning brings this surface near the CCD wells and minimizes the extent of lateral diffusion. This increases MTF and decreases crosstalk between pixels. Thinning, however, lowers the responsivity for wavelengths greater than about 0.8μ.

(2) Accumulation. An unoxidized silicon surface is a region of rapid electron recombination. Signal electrons that recombine at the back surface are not detected by the CCD. Since most signal electrons generated by energetic radiation are created near the back surface, this recombination must be inhibited to achieve adequate response. This is accomplished by building into the silicon substrate an electric field that forces signal electrons away from the back surface. The electric field is generated by enhancing the boron doping density of the silicon at the surface compared to

the bulk doping density. Since boron atoms in silicon are negatively charged, this accumulation of boron introduces a fixed space charge that repels signal electrons from the silicon surface.

The magnitude E of this field is given by:

$$E = \frac{kT}{q} \frac{d}{dx} [\ln N_B(x)] \qquad (1)$$

where k = Boltzman's constant

T = temperature (°K)

q = electronic charge

$N_B(x)$ = boron concentration profile

(3) Bonding. Backside illumination requires a header which provides for frontside bonding and backside imaging. For intensification applications, the header must be compatible with vacuum processing and with photocathode formation.

This paper discusses the results of the processing developed to meet these requirements.

II. Analysis

Prior to discussion of the processing results, an analysis of the backside structure will be given for the case of photon illumination. In order to simplify the analysis, several assumptions about the structure will be made. It will be assumed that:

(1) The bare silicon surface is a region of high electron-hole recombination, characterized by a surface recombination velocity, S ;

(2) the boron accumulation layer produces a uniform electric field extending from the surface to the edge of the depletion region; and

(3) the minority carrier diffusion length in the bulk away from the surface is sufficiently long that recombination (R) in the bulk can be neglected compared to surface recombination. These assumptions are summarized in Figure 1.

The quantum efficiency and dark current characteristics of this structure can be calculated by solving the continuity equation for electrons,

$$D\frac{d^2n}{dx^2} + \mu E\frac{dn}{dx} + \alpha N e^{-\alpha x} - \frac{n-n_o}{\tau} = 0 \ , \qquad (2)$$

where n = electron density,

D = electron diffusivity,

μ = electron mobility,

E = electric field,

α = silicon absorption coefficient,

N = incident photon flux,

n_o = equilibrium electron concentration, and

τ = electron lifetime.

For this analysis it will be assumed that E is a constant. Although E is actually a function of x unless $N \sim e^{\pm x}$, the additional mathematical complexity does not add to the basic understanding. The actual value of E used will be an average for the entire accumulation region. The spatial variation of n_o will be ignored.

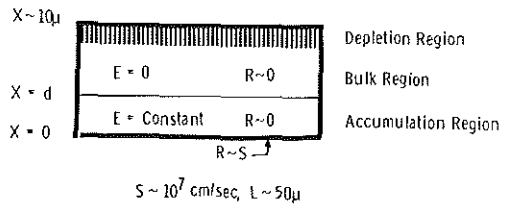

Figure 1

Similar analyses have been reported[6,7], which employ the parameters of several layers within the silicon to describe the measured spectral response. The results presented here reproduce the wavelength dependence of this response using a single measured device parameter and the measured optical constants of silicon.

The boundary conditions needed to solve Equation (2) are determined by the recombination at the back surface and by the diffusion of electrons into the CCD depletion region at the front side. The first condition yields

$$D\frac{dn}{dx} = S(n-n_o) \quad \text{at } x = 0; \tag{3}$$

the second yields

$$n = 0 \quad \text{at } x = d, \tag{4}$$

where $x = 0$ is the back surface, and $x = d$ is the edge of the CCD accumulation region. This last equation is equivalent to assumption 3.

Equation (2) is easily solved subject to the boundary conditions (3) and (4). The electron current into the CCD is then obtained by adding the electron drift current and diffusion current at $x = d$:

$$I = D\frac{dn}{dx} - \mu En \quad \text{at } x = d. \tag{5}$$

The quantum efficiency is the ratio of the photoelectron current to the photon flux, reduced by reflection losses:

$$QE = (1-r)(1/N)(I-I_D) \tag{6}$$

where I_D is the dark current and r is the reflection coefficient.

The algebraic complexity of the resulting expressions is simplified by assuming an electric field magnitude such that

$$E > \frac{6kT}{q}\frac{1}{D\tau} \tag{7}$$

For a 1 μs lifetime and $D = 5$ cm^2/s, this implies an electric field greater than 60V/cm.

From this assumption one obtains

$$I = \{q/(1 + S/\mu E)\}\{n_o S + [N/(D\alpha + \mu E - 1/\alpha\tau)]$$

$$[\mu E + S + D\alpha - e^{-\alpha d}(\mu E + S + \alpha D + S\alpha D/\mu E)]\} \tag{8}$$

Additional simplification results from a comparison of the magnitude of each term. S is assumed to be a maximum equal to the electron thermal velocity of 10^7 cm/s. The diffusivity value and mobility were assumed to be high concentration values[9]. The absorption coefficients were obtained from published results[10]. For values of E less than 5000V/cm, it was found that $D\alpha < 4 \times 10^5$ cm/s, $\mu E < 1 \times 10^6$ cm/s, and $1/\alpha < 10^4$ cm/s. Therefore, neglecting the small terms, equation 8 becomes

$$I = q\{\mu En_o + N/(1 + D\alpha/\mu E) - Ne^{-\alpha d}\} \tag{9}$$

Using the relationship $D = \mu kT/q$, one obtains

$$I = q\mu En_o + qN(1 + kT\alpha/qE) - qNe^{-\alpha d} \tag{10}$$

The quantum efficiency predicted by Equation (10) is determined using Equation (6) with $I_D = \mu En_o$. The result is

$$Q.E. = [1 - r]\{[1/(1 + kT\alpha/qE)]-e^{-\alpha d}\} \tag{11}$$

The quantum efficiency is seen to be limited by reflection losses (1 - r), transmission losses ($e^{-\alpha d}$), and recombination losses. The recombination term involves the ratio of the thermal voltage, kT/q, and a voltage defined by the electric field and the absorption coefficient. This suggests the mechanism for the wavelength dependence of Equation (11). When an electron is generated at a distance x from the back surface, a potential difference of E times x exists between x and the back surface. If E times x is less than the thermal voltage, kT/q, significant recombination can occur. E times $1/\alpha$ represents an average potential difference.

For longer wavelengths, not all photons will be absorbed in the field region, $x < d$. The $e^{-\alpha d}$ term in equation (11) represents these photons. Some of these photons will be absorbed, however, in the region $x > d$ and will contribute to the quantum efficiency. To account for this it will be assumed that all of these photons are absorbed and that all resulting electrons are collected by the CCD. This, in effect, removes the $e^{-\alpha d}$ term from the quantum efficiency equation. This assumption will be valid for sufficiently high bulk lifetime and for wavelengths which are completely absorbed in $\sim$ 10 microns. This limits the validity of the assumption to wavelengths of less than 0.9μ. For longer wavelengths, multiple reflections occur which complicate the analysis.

Equation (11) is plotted in Figure 2 (with the $e^{-\alpha d}$ term deleted) with the field,

E, as a parameter. The quantum efficiency is strongly dependent on E for fields less than 5000V/cm. Above this value, reflection limited response is approached.

The dark current generated at the back surface can also be determined from Equation (8) by evaluating Equation (5) at x = 0 with N = 0 (no illumination). The results are:

$$I_{DC}(x = 0) = qn_o S/(1 + S/\mu E) \qquad (12)$$

For the case considered above, S > μE, this equation becomes

$$I_{DC}(x = 0) = q\mu n_o E \qquad (13)$$

In order not to degrade the CCD dark current characteristics, this current must be negligible.

At first glance the field dependence of the quantum efficiency (Equation 11) and the dark current (Equation 13) appear to be inconsistent; both Q.E. and dark current increase with E. However, the dark current is also proportional to n_o. Both n_o and E are related to the boron concentration at the surface:

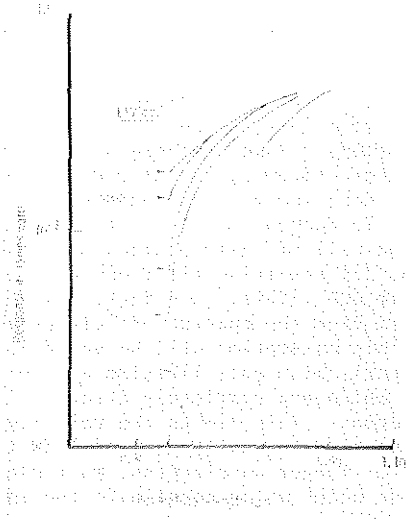

Figure 2

$$n_o = n_i^2/N_B \qquad (14)$$

and

$$E = \frac{kT}{q}\frac{d}{dx}(\ln N_B) \sim \frac{kT}{q}\frac{1}{d} \qquad (15)$$

To first order, E is independent of N_B, while n_o decreases with N_B. This allows a proper choice of accumulation parameters so that the field can be maximized while n_o is reduced, resulting in high quantum efficiency without increased dark current.

The results of this analysis will be compared to experimental results in the following sections.

III. Processing Results

(A) Thinning. After completion of slice processing and multiprobe evaluation, the imagers are thinned to the desired membrane thickness. The thinning results are illustrated in Figure 3. This figure shows a two-inch silicon slice into which 0.4 inch square membranes have been etched. The membrane is approximately 10 microns thick, allowing the transmission of red light. The dark frames around each membrane are provided for support.

Thickness non-uniformities cannot be detected visually. The uniformity can best be determined by an optical interference technique. This employs infrared radiation which is only weakly absorbed by the silicon. Incoming and reflected radiations interfere, producing fringes in the imager response. This is illustrated in Figure 5, which shows the video display of the output of an imager illuminated from the rear with 1.1 micron narrow band ($\Delta\lambda$ = 16Å) radiation. Each fringe represents a region of constant thickness. The thickness variation between adjacent fringes is given by

$$\Delta d = \frac{\lambda}{2N} \qquad (16)$$

where λ = 1.1 microns and N = 3.4. The thickness variation indicated in Figure 4 is about 0.3 micron. The active area of this imager is 0.9 cm x 0.7 cm. This thickness variation therefore corresponds to a taper of approximately 0.005 degrees.

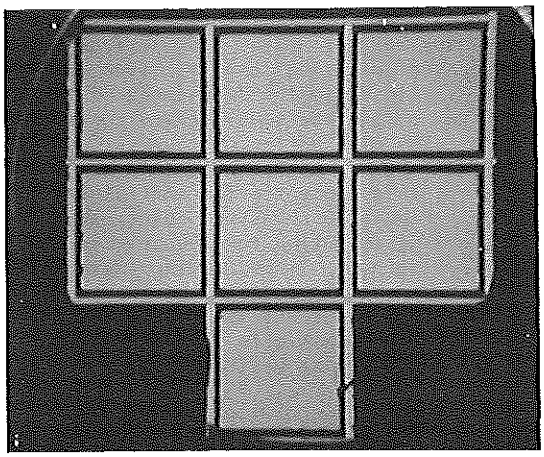

Figure 3

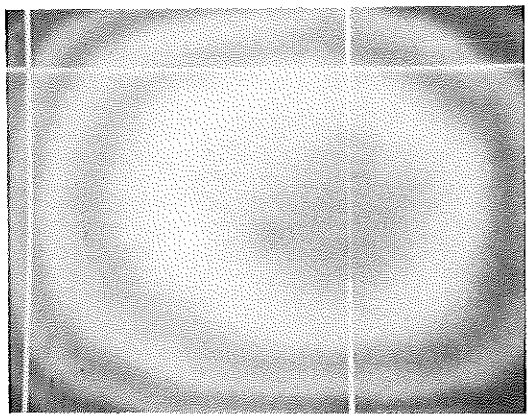

Figure 4

Membranes as large as 1.2 cm square have been produced without difficulty.

An imager parameter associated with the membrane thickness is the modulation transfer function (MTF). MTF curves at 0.4 micron illumination for thinned imagers with 22.9 micron square pixels are shown in Figure 5.

(B) Accumulation. The results of the Texas Instruments accumulation process are illustrated in Figure 6. This shows the spectral response characteristics of sixteen 100 x 160 devices. The average and standard deviation at each wavelength is shown. These devices were not selected for high spectral response; the results indicate the normal spread in response obtained from the process.

Another parameter directly affected by the accumulation process is the electron gain during intensified operation. This is defined as the ratio of the CCD output current to the incoming accelerated electron current. The results of gain measurements on seven completed ICCDs are summarized in Figure 7. The reproducibility illustrated in Figure 6 is also evident here.

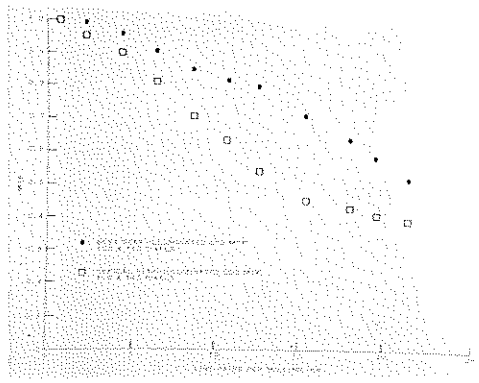

Figure 5

In order to compare the spectral response results to the analysis reported earlier, the average electric field in the accumulation region was determined by making boron concentration profile measurements. It was determined that the average field was approximately 400V/cm. Equation (11) was evaluated using this field for wavelengths from 0.4μ to 0.8μ. In Figure 8 the results are compared to the measured response. It can be seen that the analysis predicts the wavelength dependence rather well, but the

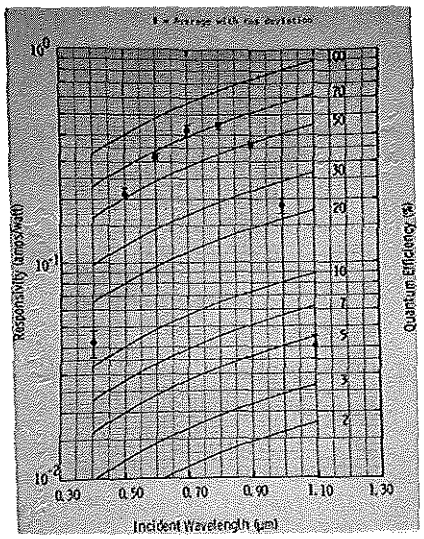

Figure 6

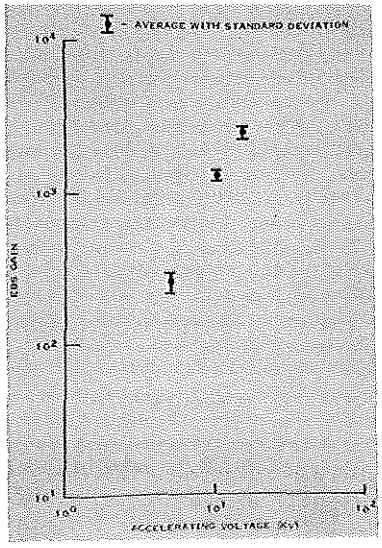

Figure 7

calculated magnitude is less than the measured response. The ratio of the calculated response to measured response is 81 percent plus or minus 6 percent from 0.5μ to 0.8μ. The source of this magnitude discrepancy is under investigation.

The dark current predictions of Equation 13 were verified by determining the CCD dark current versus back surface boron concentration. The results, given in Figure 9, illustrate the dependence of the dark current on the backside surface concentration. The elimination of rear-surface-generated dark current can be achieved by maintaining this concentration sufficiently high. Figure 10 shows the resulting dark current distribution for the devices reported in Figure 5. (These devices were selected from a set of completed devices on the basis of dark current magnitude; the data presents the achievable dark current magnitude and its relative frequency of occurrence.

(C) Packaging. Thinned imager arrays require special packages which allow frontside bonding and backside illumination. Figure 11 illustrates a package employed in intensified charge coupled device operation. Several problems were initially encountered in implementing these packages:

1. low package fabrication yield;
2. chip attachment to the package can cause membrane buckling or fracture;
3. gold wire bonding to aluminum bond pads leads to "purple plaque."

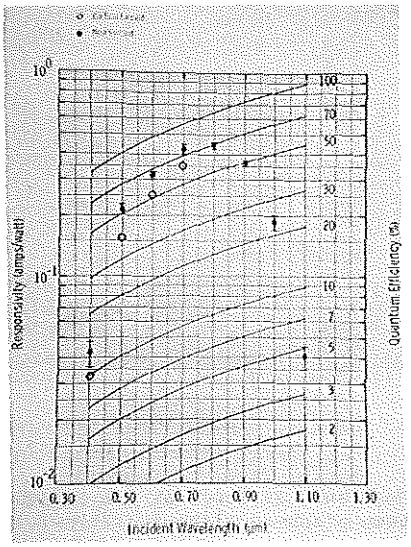

Figure 8

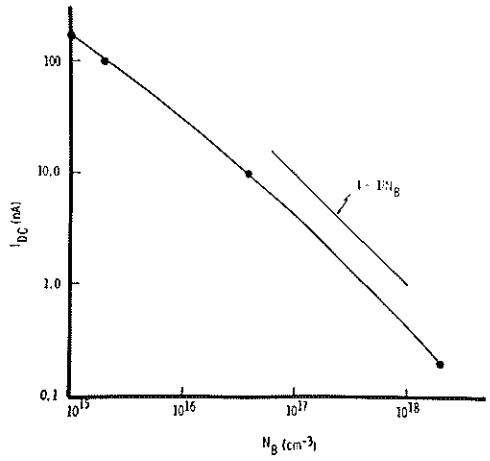

Figure 9

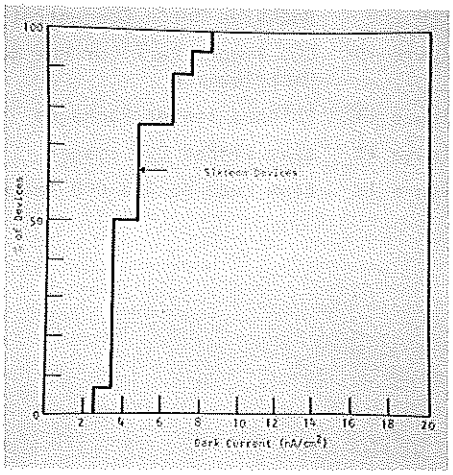

Figure 10

To eliminate some of these problems, gold beam lead bonding has been developed for thinned imagers. This allows the bonding of imagers with the frontside down--significantly reducing the required complexity of the package. In addition the beam leads tend to isolate the membrane from the thermal stresses introduced by the package, eliminating buckling. Figure 12 shows an imager with beams added to the bond pads. Figure 13 shows a completed imager beam-lead bonded to a flat ceramic substrate.

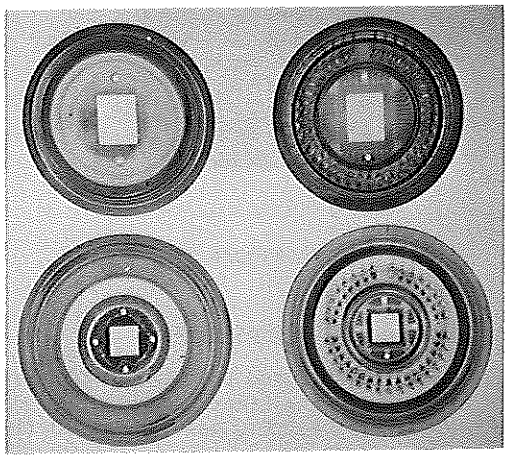

Figure 11

III. Conclusion

The processing of imagers for backside illumination has been developed to the point that reproducible spectral response, EBS gain, and dark current results are obtained. A simple theory has been developed which predicts the wavelength dependence of the spectral response using only measured parameters. The theory also predicts the observed dependence of the dark current on the backside surface concentration. The resultant understanding of the process effects on the spectral response (and EBS gain) allows further development toward reflection-limited quantum efficiency.

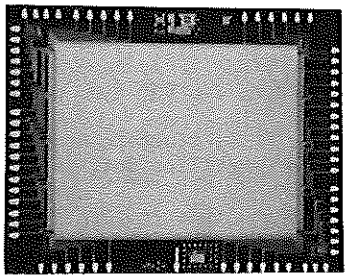

Figure 12

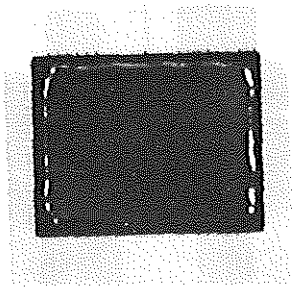

Figure 13

References

1. Caldwell, L., and Boyle, J., "Operation of CCDs in the Electron Bombarded Mode," Proc. of S.P.I.E., Vol. 78, p. 10 (1976).

2. Sobieski, S., "Intensified Charge Coupled Devices for Ultra Low Light Level Imaging," Proc. of S.P.I.E., Vol. 78, p. 73 (1976).

3. Zucchino, P., and Lowrance, J.L., "ICCD Imaging Detector for Plasma Physics Instrumentation," presented at the 7th Symposium on Photo-electronic Image Devices, London, 1978.

4. Woodgate, B., private communication.

5. Antcliffe, G. A., et. al., "A Backside Illuminated 400 x 400 Charge Coupled Device Imager," IEEE Trans. Electron Devices, Vol. ED-23, p. 1225 (1976).

6. Buck, T.N., et. al., "Influence of Bulk and Surface Properties on Image Sensing Diode Arrays," Bell Syst. Tech. J., Vol. 47, p. 1827 (1968).

7. Crowell, M.H., and Labuda, E.F., "The Silicon Diode Array Camera Tube," Bell Syst. Tech. J., Vol. 48, p. 1481 (1969).

8. Harten, H.U., "Surface Recombination of Silicon," Phillips Res. Rep. 14, p. 346 (1959).

9. Grove, A.S., Physics and Technology of Semiconductor Devices, John Wiley and Sons, Inc., New York, 1967.

10. Phillip, H.R., and Taft, E.A., "Optical Constants of Silicon in the Region 1 to 10 eV," Phys. Rev. 120, 37 (1960).

List of Figures